Solid State Phenomena
ISSN: 1662-9779, Vol. 389, pp 207-215
doi:10.4028/p-kh92Rm

Submitted: 2026-01-19
Revised: 2026-02-18
Accepted: 2026-02-24
Online: 2026-04-16

Experimental and Numerical Investigation of AA6061 Tube Flowformability

Katia Mocellin[1,a*], Nagasai Meghana Rani Kauta[1,b] and Pierre-Olivier Bouchard[1,c]

[1]Mines Paris, Université PSL, Centre de Mise en Forme des Matériaux (CEMEF), UMR CNRS, 06904 Sophia Antipolis, France

[a*]katia.mocellin@minesparis.psl.eu, [b]meghanakns@gmail.com, [c]pierre-olivier.bouchard@minesparis.psl.eu

Keywords: flowforming, tube flowformability, AA6061, finite element simulation.

Abstract. This study introduces a novel flowformability test aimed at replicating the complex loading conditions of industrial flowforming processes-alternating stress triaxiality, large plastic strains, and high strain rates. A novel Conical Flowformability Test (CFT) configuration was selected for experimental validation due to its ability to achieve a high theoretical thickness reduction while respecting machine constraints. Experiments conducted on AA6061 in O-temper and W+3h states demonstrated substantial thickness reductions. Comparison between the numerical simulations using the software FORGE® and the experimental results is satisfactory despite certain unquantifiable experimental defects such as fish scales and material build-up. The current study paves way to establish a robust framework for assessing material flowformability and damage evolution under realistic process conditions.

1. Introduction

Flowforming is a near-net-shape manufacturing process widely used for producing high-performance tubular and conical components in aerospace, defense, and energy sectors. Its major advantage lies in achieving large plastic strains under controlled incremental deformation, resulting in superior mechanical properties and dimensional accuracy [1]. However, the process imposes highly complex loading paths characterized by alternating positive and negative stress triaxiality, very high strain rates, and severe plastic deformation [2]. These conditions complicate damage prediction, as conventional material characterization tests—such as tensile, compression, or torsion tests—are unable to replicate the incremental and non-proportional loading inherent in flow forming; moreover, these tests tend to predict final fracture at plastic strain levels significantly lower than those typically attained during flowforming.

Several mechanical tests have been proposed in the literature to evaluate ductile fracture under conditions approaching those encountered in flow forming. Common approaches include conventional tensile tests [3], in-plane torsion tests [4], and TELE test [5], which aim to correlate fracture strain with stress state parameters such as triaxiality and Lode angle. While the conventional tests provide valuable insights for monotonic or proportional loading, they fall short in reproducing the cyclic stress state and alternating triaxiality observed in flowforming. On the other hand, in-plane torsion tests reproduce very large strains and cyclic loading while lacking to produce non-proportional alternate tensile – compressive loading.

To address these limitations, a dedicated damage test is required—one that can mimic the essential features of flowforming:

- *Alternating stress triaxiality* (compressive under roller contact, tensile during material flow),
- *Large plastic strain accumulation* over multiple tool passes, and
- *High strain rates* induced by combined rotation and axial feed.

Such a test should also provide a measurable experimental observable-typically the final thickness at fracture-linked to flowformability or spinnability as discussed in [6], [7]. This observable serves as a practical indicator for process design and material selection.

In this context, the present work introduces a novel *Conical Flowformability Test (CFT)*, specifically designed to replicate flowforming conditions under laboratory constraints. Unlike conventional tube flowformability tests, which require radial roller motion, the CFT adapts to the axial-only roller movement of the laboratory FluoTi device by modifying the preform and mandrel geometry. This configuration enables high thickness reduction ratios (up to 80%) while respecting machine limitations, thereby providing a robust platform for experimental damage characterization and numerical validation. The following sections detail the experimental setup, modelling approach, and hybrid methodology adopted to evaluate flowformability and identify critical damage thresholds.

2. Methodology

2.1 Conceptual Design

The laboratory Fluoti test device (see Fig. 1) has certain limitations with respect to flowformability testing. Conical Flowformability Test (see Fig. 2) was selected because it can reach high thickness reductions (TR) up to 80% while remaining compatible with these limitations. Flowformability (TR_{max}) which is the maximum thickness reduction that can be obtained before failure of the specimen, can be mathematically defined as seen in Eq. 1, where e_0 and e_f are the initial and final specimen thickness respectively.

$$TR_{max} = \frac{e_0 - e_f}{e_0} \times 100 \tag{1}$$

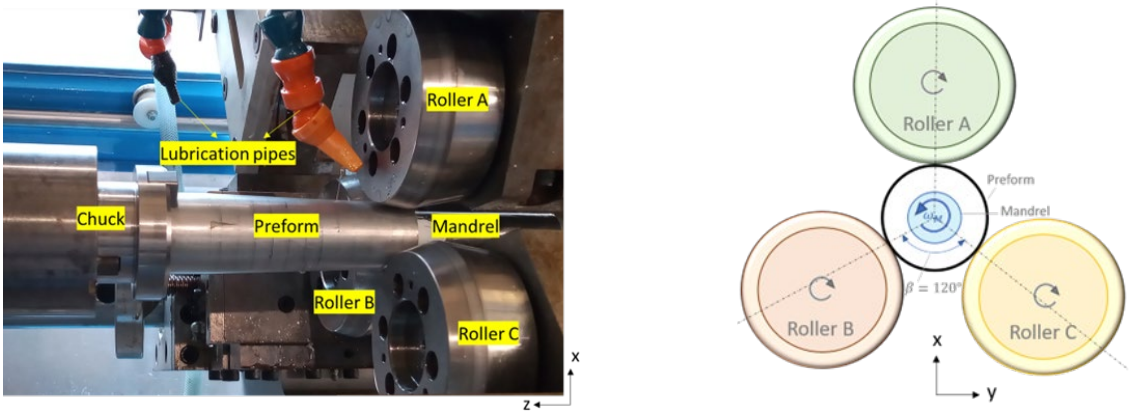

(a) (b)

Fig. 1. FluoTi machine set up (a) Experimental, (b) Schematic representation.

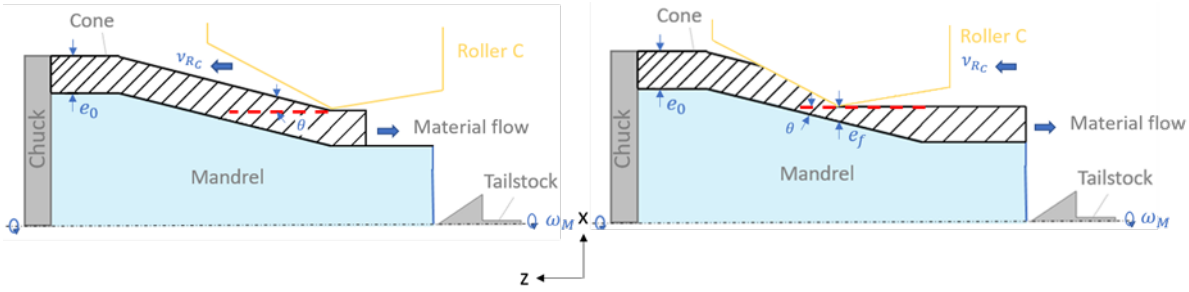

Fig. 2. Schematic representation of CFT in its initial (left) and final (right) stages.

2.2 Experimental Setup

The conical preform is mounted on the cylindrical mandrel and fixed in position using sockets. The rollers are then adjusted so that their tips are positioned at the desired positions as shown in Fig.3. Distances between the tips of the three rollers are $\boldsymbol{d_{bc}} = 3.44$ mm and $\boldsymbol{d_{ac}} = 6.44$ mm. The reference

roller chosen for the experiments is Roller A. It is adjusted axially such that the tip of the roller aligns with the starting point. The other two rollers are adjusted according to the distance indicated in Table 1.

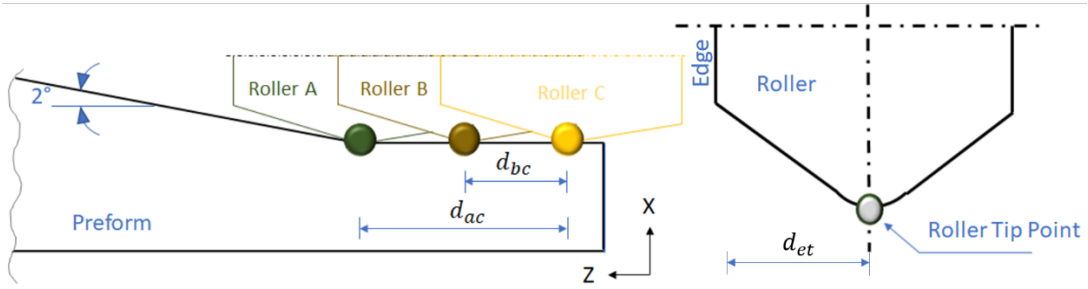

Fig. 3. Illustration of axial distance between rollers (left) and roller tip point (right).

Mandrel rotational speed was set to 205 rpm and roller feed ratios varied between 0.1 and 0.3 mm/tr. Further, the test is performed on two material states of the preform - AA6061 alloy in O-temper (mat-O) and solution-treated and 3 hour-aged state (mat-W+3h). The true stress-strain curves of these two states have been evaluated from force-displacement curves obtained using simple compression tests. This material testing methodology is presented in detail in [8].

At the end of each experiment, thickness profiles, roller forces and torque were measured and failure locations were identified visually.

2.3 Numerical Modelling

Simulations were performed in FORGE® NxT 3.1 using a Classic Lagrangian formulation. To reduce CPU time, the preform geometry consists of a 90° symmetrical geometry configuration. A comparative simulation study between 90°, 120° and 360° symmetry geometry configurations is made in [9] and shows that symmetry planes can be introduced to significantly reduce CPU time.
The material behaviour law parameters used in the simulation studied in this section are based on the Johnson-Cook (J-C) phenomenological material behaviour law given by Eq. 2. The identified J-C law parameters for mat-W+3h specimen are given in Table-1. During the process, self-heating in the deformed part is considered by means of the thermomechanical material behaviour law. In addition, the friction law used is given in Eq. 3 with the friction law parameters of $\bar{m}$=0.4 and μ=0.2. The experiment is carried out at ambient temperature conditions. Important simulation outputs include thickness evolution, roller forces and local damage metrics.

$$\sigma = [\sigma_0 + K\bar{\varepsilon}^n]\left[1 + C\ln\frac{\dot{\bar{\varepsilon}}}{\dot{\bar{\varepsilon}}_0}\right]\left[1 - \left(\frac{T - T_0}{T_m - T_0}\right)^m\right] \quad (2)$$

Where σ is the equivalent stress, σ_0 corresponds to yield stress, $\bar{\varepsilon}$ and $\dot{\bar{\varepsilon}}$ are respectively the plastic strain and strain rate, T the temperature, $\dot{\bar{\varepsilon}}_0$ and T_0 are respectively a reference (or base) temperature and a reference strain rate. T_m is the material melting temperature. C is an experimentally determined parameter considering the strain rate effect, n is the strain-hardening exponent, m is a strain rate sensitivity and K is a parameter determined experimentally.

Table 1. Johnson Cook law parameters for mat-W+3h state.

$\boldsymbol{\sigma_0}$ [MPa]	K [MPa]	n	C	m
65.58	261.5	0.27	$\mathbf{7.10^{-4}}$	1.09

$$\tau_{fr} = \min(\mu\sigma_n; -\bar{m}\frac{\sigma_0}{\sqrt{3}}) \quad (3)$$

A two-tier mesh is used as part of the conical flowformability simulations as seen in [9]. The preform is meshed with two different mesh sizes of respectively 1.25- and 3-mm. Mesh zone 1 contains more refined elements as this part of the preform is directly in contact with the rollers. The mesh size of 1.25 mm is chosen based on a preliminary convergency study.

Due to very high strain magnitudes observed during the simulation, mesh elements can degenerate. Remeshing takes place at such points to avoid such mesh degeneration. At least 4 elements in the part thickness below the roller is maintained throughout the process.

The time step, Δt chosen for the simulations is based on the condition that the distance travelled by the roller at the given rotational velocity, ω_M during the time step Δt does not exceed the length of the mesh element in the orthoradial direction, e_θ. The expression is given in Eq. 4.

$$\Delta t < \frac{e_\theta}{\omega_M} \tag{4}$$

The simulations are run on 12 CPUs of a calculation computer[1]. For the given numerical and process parameters, the computation time taken for each simulation case is nearly 40 h.

3. Results

3.1 Experimental Observations

Maximum thickness reduction before fracture was achieved approximately 78% for mat-O and 68% for mat-W+3h. Failure modes included pile-up and macro-cracking (mat-O) and fish-scale defects with macro-cracks near Roller C (mat-W+3h) as can be seen in Fig. 4.

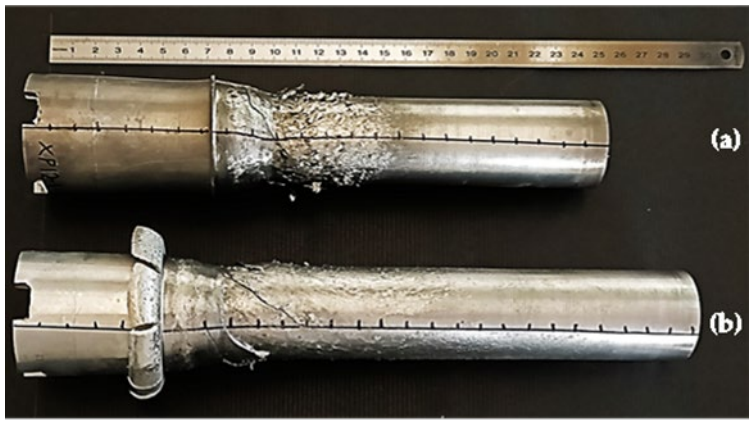

Fig. 4. Deformed parts at the end of CFT experiments on (a) mat-W+3h and (b) mat-O specimens.

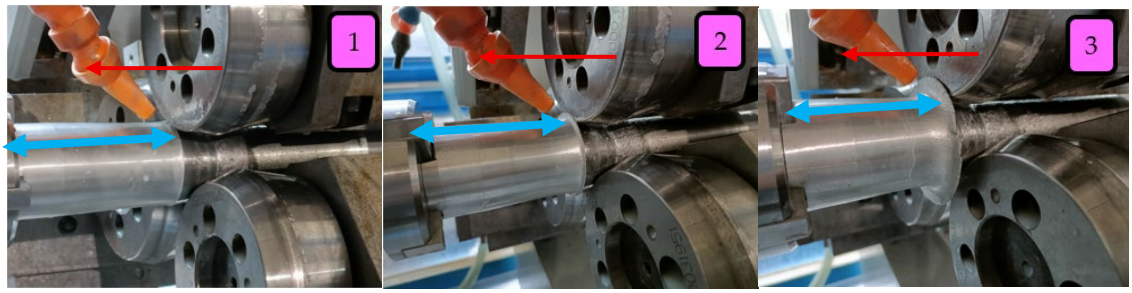

Fig. 5. Evolution of material pile-up at the three specific stages- 1 (initial), 2 (intermediate), 3 (final) for Mat-O. Blue double arrow represents the distance from the reference roller to the fixed end of the part; Red arrow, the displacement vector of the roller during the process.

Failure on the specimens can be tracked through a combination of visual inspection of the specimens and the force-displacement curves. Three stages during the conical flowformability test are shown in Fig. 5 corresponding to the respective points indicated in the force-displacement curves

in Fig. 6. The initial stage of the experiment is characterized by the near linear force-displacement experimental curve. The intermediate stage of the experiment is where the slope of the force-displacement curve increases, and the pile-up begins on the material specimen. In the final stage of the experiment, cracks are observed on the surface of specimens in both material states.

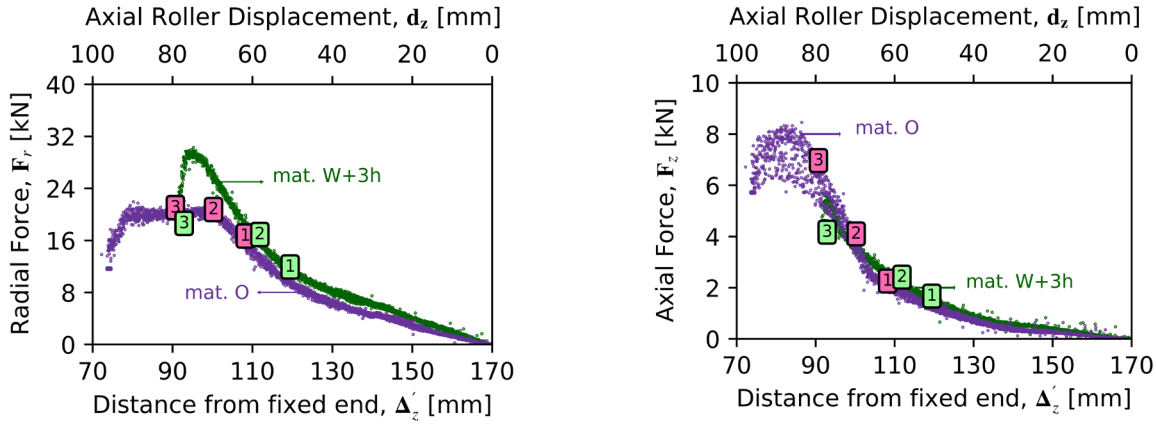

Fig. 6. Comparison of (left) radial and (right) axial roller forces obtained in the experiments on two material states, mat-O and mat-W+3h.

Mat-O being much softer than mat-W+3h, the formation of the pile-up is facilitated. This pile-up forms a collar whose diameter becomes high enough to enter in the planar vertical area of rollers as can be seen in Fig. 4 (a). This may explain the higher axial force observed for this mat-O in Fig. 6. It is indeed difficult to flow-form softer materials and rollers geometries need to be adapted accordingly. In the end, and despite the small cracks observed in the collar pile-up, final thickness reduction is higher for mat-O than for mat-W+3h, meaning higher flowformability.

3.2 Simulation vs Experiment

A material build-up is observed during the experiment as seen in Fig. 7. There is a deviation in the radial positions of the roller tips due to the material-build up in the final stage of the experiment. This difference in the radial positions of the roller tip point is evaluated between the initial and final stages of each experiment case as seen in Fig. 8. To consider this deviation, in the simulation, a linear roller trajectory in the axial direction is assumed between the experimentally measured initial and the final positions of the roller tip positions.

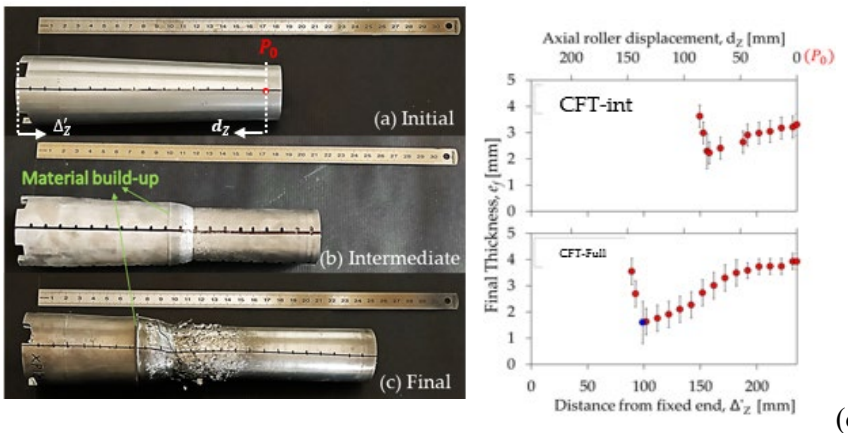

(d)

Fig. 7. Mat-O CFT specimen at (a) initial, (b) intermediate and (c) final stages of the conical flowformability experiment. In (d), experimental thickness measurements along part length at intermediate stage (upper) and at final stage (lower).

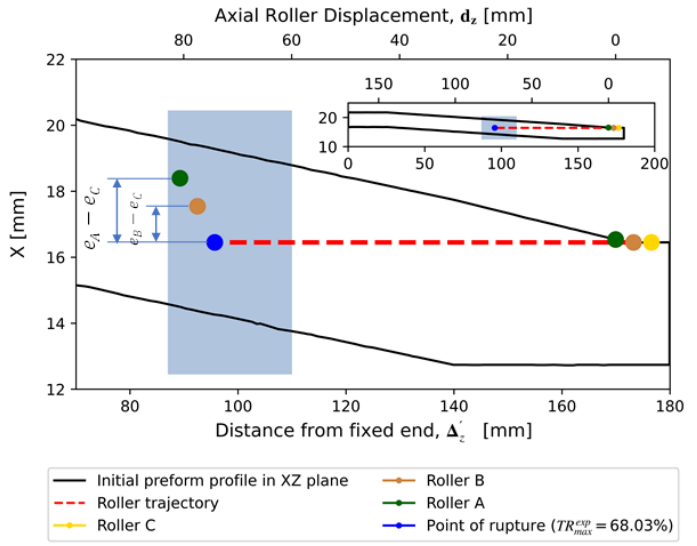

Fig. 8. Illustration of the deviation in radial tip positions of rollers A and B from C at the end of the experiment. The blue zone is the illustration of cracked zone with respect to the experiment. The dashed red line is the trajectory designed for all three rollers with their initial positions presented at the start end of the line. In the inset figure, the location of the fractured zone and final position of Roller C (in blue) are indicated with respect to the whole geometry.

The radial and axial force-displacement curves are compared between simulation and experiment for mat-W+3h specimen in Fig. 9. Axial roller displacement, d_Z and distance from fixed end, Δ_Z' are presented on the top and the bottom horizontal axes respectively. They correspond to the axial distance covered by the rollers with respect to the starting point as shown in Fig. 7. Here, both the radial and axial forces on Roller A are perfectly represented by the force curves from simulation until d_Z=30 mm. Further, points 1 and 2 on the experimental curve correspond to the points at which the axial roller displacement magnitudes are equal to $d_z = 60mm$ and $d_z = 75mm$ respectively. At point 1, the radial force is underestimated by 5.25 kN which represents an error of approximately 32%. At the same point, the axial force is underestimated marginally by 0.29 kN with respect to the experiment.

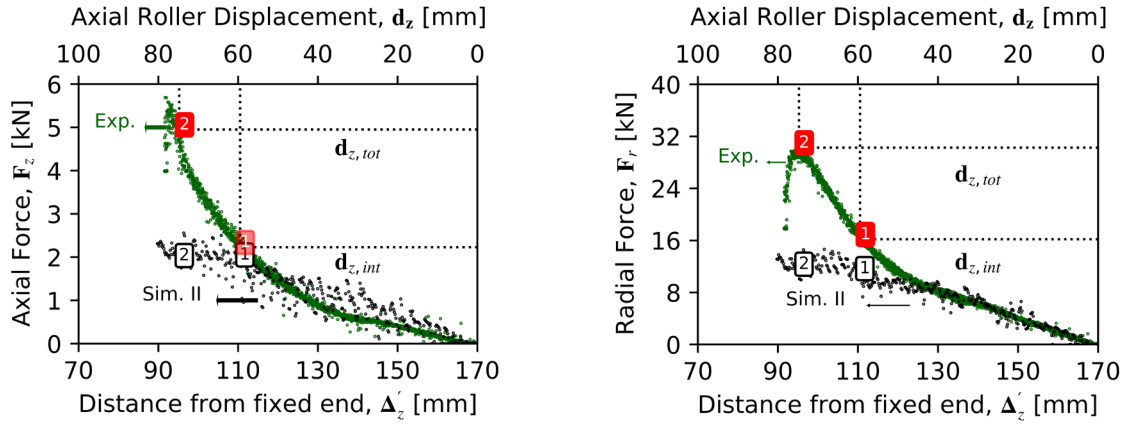

Fig. 9. Comparison of (left) axial and (right) radial Roller A forces in simulation (Sim. II) with experimental values. Point 1 and Point 2 correspond to the intermediate and the end stages of experiment on mat-W+3h specimen.

The part profiles and thickness distribution along their length at these points are compared in Fig. 10. The thickness under Roller A corresponds well with the experimental value at point 1. But at point 2, the thickness under Roller A is overestimated by 0.4 mm in the simulation which is equal to about 12% error with respect to the average value of the experiment. However, this value is within the error range of 0.5 mm calculated based on experimental measurements. As a reminder, despite the horizontal roller trajectory, the experimental thickness measurements decrease with increase in the axial roller displacement, d_z due to the conical mandrel geometry.

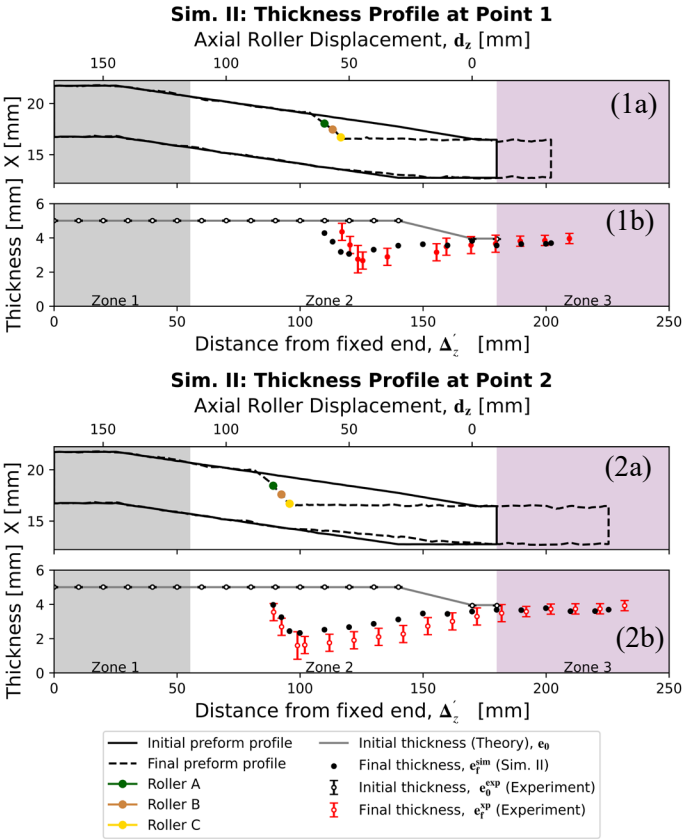

Fig. 10. In (1a) -(1b), Deformed part profile at initial and at $d_z = 60$ mm obtained from simulation (upper). Comparison of thickness in CFT-int experiment and during simulation at $d_z = 60$ mm along part length (lower). In (2a) -(2b), preform profile at initial and at $d_z = 75$ mm obtained from simulation (upper). Comparison of thickness in CFT-int experiment and during simulation at $d_z = 75$ mm along the part length (lower).

Thickness profiles were predicted accurately in regions dominated by Roller A. Discrepancies in roller force magnitudes are attributed to machine stiffness and friction parameter uncertainties. In addition, a better understanding of phenomena such as fish-scale formation and material build-up is required. Further research on material behavior testing and identification methodologies, capable of accounting for very large strains and strain rates, would help improve these predictions. The flowformability magnitude evaluated for the two material states at the two different stages of the test is presented in Fig. 11.

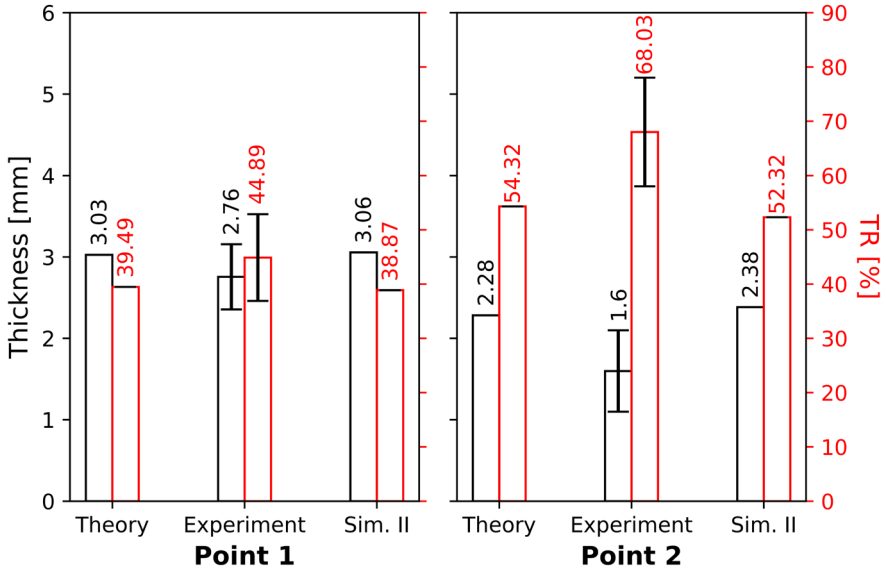

Fig. 11. Comparison of theoretical, experimental and prediction of simulation of TR_{max} (red) and final part thickness at fracture, e_f^{rup} (black).

4. Discussion and Conclusion

The proposed novel Conical Flowformability Test (CFT) demonstrates its capability to reproduce the alternating stress states and significant strain accumulation characteristic of flowforming, while remaining compatible with the laboratory FluoTi experimental device capabilities. The hybrid experimental–numerical flowformability testing helps in providing a robust framework for damage evaluation under realistic process conditions in the future. Nevertheless, the study acknowledges limitations related to machine stiffness characterization, friction law calibration, and the accuracy of predicted roller trajectories, which influence the reliability of force and thickness predictions. Furthermore, phenomena such as fish scale formation and material build-up, observed experimentally, require deeper investigation to enhance predictive accuracy. Despite these limitations, the proposed approach constitutes a significant advancement in reliable flowformability testing assessment and sets a strong foundation for a future study on ductile fracture characterization, offering a foundation for future research aimed at refining damage models and improving process simulations across a broader range of kinematic configurations.
Future work on flowformability testing should focus on:

- **Quantifying machine frame stiffness** and integrating its effect into simulation models to improve roller force prediction.
- **Developing advanced friction calibration procedures** for more accurate representation of contact conditions.
- **Investigating surface phenomena** such as fish scales and material pile-up through dedicated experimental and numerical studies.
- **Applying the methodology to ductile damage models** and multi-parameter fracture criteria for enhanced predictive capability.
- **Validating the approach across different geometries and material states** to ensure applicability to industrial flowforming processes.

Acknowledgement

This work was carried out at CEMEF, Mines Paris – PSL, as part of the FluoFAB project funded by BPI France.

References

[1] Wong, C. C., Dean, T. A., & Lin, J. (2003). A review of spinning, shear forming and flow forming processes. International Journal of Machine Tools and Manufacture, 43(14), 1419–1435. https://doi.org/10.1016/S0890-6955(03)00172-X.

[2] Roula, A. M., Mocellin, K., Traphöner, H., Tekkaya, A. E., & Bouchard, P. O. (2022). Influence of mechanical characterization on the prediction of necking issues during sheet flow forming process. Journal of Materials Processing Technology, 306. https://doi.org/10.1016/J.JMATPROTEC.2022.117620.

[3] Xu, W., Wu, H., Ma, H., & Shan, D. (2018). Damage evolution and ductile fracture prediction during tube spinning of titanium alloy. International Journal of Mechanical Sciences, 135, 226–239. https://doi.org/10.1016/J.IJMECSCI.2017.11.024.

[4] Yin, Q., Soyarslan, C., Isik, K., & Tekkaya, A. E. (2015). A grooved in-plane torsion test for the investigation of shear fracture in sheet materials. International Journal of Solids and Structures, 66, 121–132. https://doi.org/10.1016/J.IJSOLSTR.2015.03.032.

[5] Bourgeon, L. (2009). Etude et modélisation des mécanismes d'endommagement en forge à froid [Doctoral dissertation, Ecole Nationale Supérieure des Mines de Paris]. https://theses.fr/2009ENMP1671.

[6] Ma, H., Xu, W., Jin, B. C., Shan, D., & Nutt, S. R. (2015b). Damage evaluation in tube spinnability test with ductile fracture criteria. *International Journal of Mechanical Sciences*, *100*, 99–111. https://doi.org/10.1016/J.IJMECSCI.2015.06.005.

[7] Bylya, O. I., Khismatullin, T., Blackwell, P., & Vasin, R. A. (2018). The effect of elasto-plastic properties of materials on their formability by flow forming. *Journal of Materials Processing Technology*, 252, 34–44. https://doi.org/10.1016/J.JMATPROTEC.2017.09.007.

[8] Kauta, N. (2024). Analysis and modelling of flowformability through a hybrid experimental-numerical approach. [Doctoral dissertation, Ecole Nationale Supérieure des Mines de Paris]. https://theses.fr/2024UPSLM061.

[9] Kauta, N. M. R., Bouchard, P.-O., & Mocellin, K. (2022). Relevance of Symmetry Assumptions in the 3D Numerical Modeling of a Flowformability Test. Key Engineering Materials, 926, 776–783. https://doi.org/10.4028/p-07aps3.

[10] Tekkaya, A. E., Bouchard, P.-O., Bruschi, S., & Tasan, C. C. (2020). Damage in metal forming. CIRP Annals, 69(2), 600–623. https://doi.org/10.1016/J.CIRP.2020.05.005ϕ.